Structure and Sediment Budget of Yinggehai-Song Hong Basin, South China Sea: Implications for Cenozoic Tectonics and River Basins Reorganization in Southeast Asia

Chao Lei[a], Jianye Ren[a], Pietro Sternai[c], Matthew Fox[d], Sean Willett[b], Xinong Xie[a], Peter D. Clift[e], Jihua Liao[f], Zhengfeng Wang[g],

a. Key laboratory of Tectonics and Petroleum Resources of Ministry of Education, China University of Geosciences, Wuhan 430074, China

b. Department of Earth Sciences, ETH Zürich, CH-8092 Zürich, Switzerland

c. Division of Geological and Planetary Sciences, California Institute of Technology, Pasadena, CA 91125, USA

d. Department of Earth and Planetary Science, University of California, Berkeley, USA and Berkeley Geochronology Center, Berkeley, USA.

e. Department of Geology and Geophysics, Louisiana State University, Baton Rouge, LA 70803, USA

f. China National Offshore Oil Corporation Ltd., Beijing 100010, China

g. China National Offshore Oil Corporation Ltd., Zhanjiang 524057, China

Abstract: The temporal link between offshore stratigraphy and onshore topography is of key importance for understanding the long-term surface evolution of continental margins. Here we present a grid of regional, high-quality reflection seismic and well data to characterize the basin structure. We identify fast subsidence of the basin basement and a lack of brittle faulting of the offshore Red River fault in the Yinggehai-Song Hong basin since 5.5 Ma, despite dextral strike-slip movement on the onshore Red River fault. We calculate the upper-crustal, whole-crustal, and whole-lithospheric stretching factors for the Yinggehai-Song Hong basin, which show that the overall extension observed in the upper crust is substantially less than that observed for the whole crust or whole lithosphere. We suggest that fast basement subsidence after 5.5 Ma may arise from crustal to lithospheric stretching by the regional dynamic lower crustal/mantle flow originated by collision between India-Eurasia and Indian oceanic subduction below the Eurasian margin. In addition, we present a basin wide sediment budget in the Yinggehai-Song Hong basin to reconstruct the sedimentary flux from the Red River drainage constrained by high-resolution age and seismic stratigraphic data. The sediment accumulation rates show a sharp increase at 5.5 Ma, which suggests enhanced onshore erosion rates despite a slowing of tectonic processes. This high sediment supply filled the accommodation space produced by the fast subsidence since 5.5 Ma. Our data further highlight two prominent sharp decreases of the sediments accumulation at 23.3 Ma and 12.5 Ma, which could reflect a loss of drainage area following headwater capture from the Paleo-Red River. However, the low accumulation rate at 12.5 Ma also correlates with drier and therefore less erosive climatic conditions.

Key words: Yinggehai-Song Hong Basin, South China Sea, Exhumation, Sediment Budget, Red River Fault

1 Introduction

The collision of India with Eurasia, starting in the late Paleocene-early Eocene (e.g. Royden, 1997; Tapponnier et al., 2001; Replumaz et al., 2013; Leech et al., 2005) and continuing to the present, resulted in the formation of the Tibetan Plateau, the highest terrain on the planet. It is widely accepted that Tibetan mountain building influenced global climate (e.g. An et al., 2001; Molnar et al., 1993; Tapponnier et al., 2001) as well as regional drainage patterns (e.g. Brookfield, 1998; Clark et al., 2004), which in turn control the discharge of eroded sediment to the ocean (e.g. Molnar et al., 1993).

The region of Southeastern Tibet, northern Vietnam and southwest China is particularly important for understanding the causative relationships between climate, erosion and tectonic changes during the Cenozoic. There are several large rivers here (e.g. Red River, Yangtze River, Mekong River and Pearl River) separated by parallel mountain ranges. The Red River has been a special focus of research because of suggestions that this drainage was much larger in the past than it is at present (Brookfield, 1998; Clark et al., 2004). According to this proposal, the Red River had been one of the largest systems in Asia, but suffering progressive loss of drainage area to the neighboring Yangtze River through the Cenozoic as a result of drainage capture. However, the time for this river capture event has been the subject of debate for more than two decades. Local geomorphological studies along the eastern margins of the Tibetan plateau show that major headwater capture from the paleo-Red River occurred before the late Miocene (Clark et al., 2004). Nd isotopes have been used as a provenance tool in the onshore Hanoi Depression and showed a rapid change of compositions towards negative value during the Oligocene, before ca. 24 Ma (Clift et al., 2006). It has also been argued on the basis of thermochronometric data that the capture of the middle Yangtze and Sichuan basin by the lower Yangtze, beheading the Red River, took place in the Eocene (Richardson et al., 2010). However, detrital zircon U-Pb ages at the lower reaches of the Yangtze River suggested that capture of middle Yangtze River occurred at 36.5-23 Ma (Zheng et al., 2013). Furthermore, zircon data from close to the 'first bend' (the apparent capture point between the Red and the Yangtze rivers) seems to suggest a re-routing of the river from the south to the northeast only 1.7 Ma ago (Kong et al., 2012). Previous studies mainly focused on the Red River estuary or the Yangtze River drainage system, but neglected the sedimentary history of the Yingghehai-Song Hong basin, which has a better age control from biostratigraphic constraints within the marine sediments.

In this study we present newly released high-resolution seismic reflection profiles and well data from the Yinggehai-Song Hong basin, located offshore of the Red River drainage (Figure 1). Based on this new data, we constrain the geology of the basin at depth and reconstruct the strike-slip movements of the offshore Red River fault. Unlike the dextral strike-slip movement of the onshore Red River fault, offshore Red River fault has been inactive and characterized by fast subsidence since 5.5 Ma. These observations cast doubt on the interpretation of the dextral strike-slip movement of the Red River fault in the Yinggehai-Song Hong basin and its controls on the basin's evolution. A high-resolution sediment budget is reconstructed for the Yinggehai-Song Hong basin, which we consider to be dominated by the Red River, an assumption consistent with our data and supported by previous multidisciplinary investigations (Shi et al., 2001; Wang et al., 2011). We use estimated accumulation rates of clastic material to infer continental erosion rates in the source area and find abrupt decrease at 23.3 Ma and 12.5 Ma respectively, and a sharp increase at 5.5 Ma. Through these results, we constrain the climatic and tectonic evolution of SE Asia and provide additional insights on potential Red River capture events.

2 Geological Setting

The Yinggehai-Song Hong basin formed at the southeastern termination of the largest Tibetan strike-slip lineaments, the Red River fault zone, and is the principal repository of material eroded from the Red River drainage. To the north it is separated from the Hanoi Depression by the structural high of the Lingao Uplift (Figure 1), while to the south and east it connects to the South China Sea. The basin contains a large thickness of Cenozoic sediments, up to 17-20 km thick (Gong and Li, 1997; Lei et al., 2011; Zhu and Lei, 2013), making the Yinggehai-Song Hong basin one of the thickest basin sections on Earth. Most of the sediments were delivered by the Red River (Wang et al., 2011; Shi et al., 2001), which currently originates in SE Tibet and SW China, running across the SW edge of the Yangtze Craton, into NW Vietnam and terminating at the Yinggehai-Song Hong basin. Thus, the sedimentary successions preserved within the Yinggehai-Song Hong basin is a source of information about the processes affecting erosion across the southeastern margin of the Tibetan Plateau and SE Asia.

Opening of the NW-trending Yinggehai-Song Hong basin has often been linked to the strike-slip motion of the Red River fault (e.g. Gong and Li, 1997; Jolivet et al., 1999; Rangin et al., 1995; Sun et al., 2003; Zhu et al., 2009), which has been proposed to have occurred in response to collision of India and Asia (e.g. Tapponnier et al., 1990 and 2001; Leloup et al., 1995 and 2001; Molnar and Tapponnier, 1975; Peltzer and Tapponnier, 1988) and/or back-arc extension associated to the Indian and other western Pacific subduction zones (e.g. Jolivet et al., 1994; Fournier et al., 2004; Taylor and Hayes, 1983; Sternai et al., 2014). However, to the east of the Yinggehai-Song Hong basin, the structures are closely related with rifting, which is associated with oceanic spreading of the South China Sea (Zhu and Lei, 2013; Clift and Sun, 2006). The initial deformation of the Red River Fault Zone was left-lateral in the Oligocene-early Miocene (Gilley et al., 2003; Leloup et al., 2001; Searle et al., 2010). It is estimated that the left-lateral displacement is 500-1400 km (e.g. Leloup et al., 2001; Tapponnier et al., 1990). The high heat flow in the basin (Gong and Li, 1997; Hao et al., 1995) may be the result of extension of the lithosphere by the mantle return flow due to rollback of the Indian and other western pacific subduction zones (Jolivet et al., 1994; Fournier et al., 2004; Sternai et al., 2014). In the Pliocene, the Red River fault changed its sense of motion to dextral strike-slip (Allen et al., 1984; Leloup et al., 1995; Replumaz et al., 2001). The magnitude of right lateral displacement, however, is much smaller and generally considered to be on the order of tens of kilometers.

3. Data and methodology

This study is based on 155 000 km of recently reprocessed regional 2D conventional reflection seismic data, kindly provided by the China National Offshore Oil Corporation (CNOOC). The 2D seismic reflection profiles cover large parts of the Yinghehai-Song Hong basin. The seismic lines in the Lingao Uplift, the Eastern Slope and the Central Yinggehai-Song Hong Depression are generally in a 5×8 km grid spacing, but denser in some areas. Two 3D seismic reflection datasets cover the structures and overlying strata of the Diapirs LD221 and DF11 (Figure 1).

Well logs in the basin were used to verify our interpretation of the depth to key horizons. Based on the amplitude and geometry of the reflections, in accordance to the method of Sangree and Widmier (1979), the Neogene succession in the basin was divided into 13 seismic units. These horizons were then correlated across the entire study area with age picks from 28 drilling sites with nannofossil biostratigraphy. The original biostratigraphic zones provided in the drilling reports were converted into numerical ages using the timescale of Walker and Geissman (2009). The oldest age from drillings was Cretaceous rocks in wells LT1135, YIN1, YIN6, YINQ2 and YX3211. However, these wells penetrated less than 1 km into the Cenozoic sediments. The well LG1120 in Lingao Uplift and well LT11A1 in central Yinggehai-Song Hong basin penetrated deeper in the section in a stratigraphic column without erosion. Age resolution is best for Miocene and Plio-Pleistocene strata because a number of wells penetrated these formations. The Oligocene strata were cored from the industrial wells LG1120 and LT11A1. In contrast, Eocene strata were not cored by industrial wells, so we could not provide a detailed temporal subdivision for these units. However, the base of Eocene strata is inferred from the basement reflector, which can be followed over long distances from the Beibuwan and Qiongdongnan basins.

Age controls are present on regional mapped seismic horizons for 55, 38, 32, 23.3, 17.5, 16.5, 15.5, 13.8, 12.5, 10.5, 5.5, 4.2, 3.8, 2.4 and 1.9 Ma. The geophysical data were interpreted using the Geoframe software produced by Schlumberger GeoQuest. After a time-depth conversion achieved by applying regional stacking velocities from the original processing of multichannel reflection data and well logging data constructed by the CNOOC, the major seismic units were converted into depth isopach maps based on a weighted least squares contouring algorithm in Landmark's Z-Map Plus.

Because most of the wells in the Yinggehai-Song Hong basin were drilled on the basement highs or on diapiric structures, sediment decompaction estimates are performed on 523 pseudo-wells, synthesized from the seismic lines (Figure 1). The synthetic wells are representative stratigraphic columns across different domains of the basin. The lithological control for each of the synthetic wells considered here was constrained by correlation with well-based age data. Knowledge of the sediment type is important to this calculation because shales experience much greater loss of porosity during burial than sandstones (Bahr et al., 2001). For the sediments we use a standard porosity-depth curve (Athy, 1930), with an initial porosity of 0.48 and a compaction coefficient between 0.51 and 0.21 to calculate the present porosity. The porosity is calculated for each lithostratigraphic unit and corresponds to a value derived from porosity-depth curves. From the present volume and porosity we calculate the volume of the eroded material. Bulk sediment volume was inferred by integrating the point wise estimates and normalizing the rates for each dated interval.

4. Seismic interpretation

4.1 Basin structure

The seismic line 0793 (Figure 2), located in the modern offshore Red River delta, shows the general extensional structures of the Yinggehai-Song Hong basin. It shows a classic pull-apart type basin with a relatively symmetrical morphology of the basement around an axis at the Lingao Uplift. Since the deepest drilling well in the Yinggehai-Song Hong basin, well LG1120 (Figure 2), only penetrated the Oligocene sedimentary rocks, the nature of the oldest sedimentary formations in the basin center cannot be defined. However, the Paleocene-Eocene terrigenous sedimentary rocks penetrated by wells in the nearby Beibuwan and Qiongdongnan basins, which can be followed over long distances and are correlated with the deepest formations in the Yinggehai-Song Hong basin by sequence stratigraphy (Gong and Li, 1997). The Paleogene age section in the Line 0793 is offset by several medium-scale faults and the fault throw of the basin basement ranges between 1.3-2 km. It is noteworthy that the amount of extension accommodated by faulting in the Paleogene sediments decreases upwards.

The total Cenozoic stratigraphic succession in the central Yinggehai-Song Hong basin is up to 17 km thick based on gravity calculations (Gong and Li, 1997). The seismic line 0755 (Figure 3) provides a large-scale regional image of the Yinggehai-Song Hong basin along its central axis, and shows the great sag forming here. Strata are subject to a general thickening southeastward from 6.1 km to 14.6 km on the seismic line 0755 along the longitudinal axis of basin, corresponding to the lithospheric flexure toward the ocean basin. It is well documented that the Lingao Uplift underwent significant extensional faulting in the Paleogene on the seismic profile 0755. However, the deep sediments before 32 Ma in the Central Yinggehai-Song Hong Depression are poorly or not defined. 5 reflection-free structures are imaged in Line 0755. The exploration drilling cored muddy sediments from these structures. In addition, these reflection-free zones are surrounded by chaotic reflection patterns related to diapirism, which disrupts the sediments in the surrounding strata (Lei et al., 2011).

Nannofossil biostratigraphy in the Yinggehai-Song Hong and Beibuwan basins provided by CNOOC shows that the oldest age for sedimentation is ca. 55 Ma. This indicates that the basin started to rift and subside at that time. The extensional faults within the pre-Cenozoic granite basement generated large accommodation space in the basin center bounded by lateral shoulders subject to erosion (Figures 2, 4 and 5). We identify rapid subsidence after 32 Ma on the seismic profiles, which is presumably caused by the sinistral movement on the offshore Red River fault (Gilley et al. 2003).

Lines 0727 and 0735 (Figures 4 and 5) present two profiles cutting across the strike of the Central Yinggehai-Song Hong Depression and show the steep basin margin that drops off sharply into the basin center. In the eastern margin of the Central Yinggehai-Song Hong Depression, the deformation occurred across the eastern branches of the offshore Red River Fault Zone, namely the Number One, Yingdong and Dongfang faults in the Chinese literature (Figure 1). These faults dip steeply to the west with offsets up to 5 km, and mainly cut the sediment cover older than 13.8 Ma. The slip rate then decreased during the middle Miocene. The offshore Red River fault in the Yinggehai-Song Hong basin appears to have been inactive after 5.5 Ma, as there is little brittle faulting in the younger sediments. Active rifting was followed by thermal subsidence since the late Miocene, creating accommodation space and trapping large volumes of sediments.

4.2 Shelf break and sedimentation

Regional seismic profile 0755 shows a double shelf break close to the Lingao Uplift, where the basement was cut by two large faults (Figure 3). This clinoform shows that more than ca. 50 km seaward migration occurred since the early Miocene. The shelf break was considerably closer to the offshore domain than its present location. The gradient of the shelf at 23.3 Ma was about 0.1-0.2°, which is three to five times steeper than at 5.5 Ma. Following the major seaward shift associated with the reflector dated at 5.5 Ma, the clinoform at Lingao Uplift continued to prograde seaward and remained high and steep. The thickness of the sediments younger than 5.5 Ma in the Central Yinggehai-Song Hong Depression is more than 2 km, which is 3 times more than on the Lingao Uplift.

A close-up image of the shelf break at Lingao Uplift from line 0738 (Figure 6a) better images the progradational clinoform. The geometry of the depositional sequences between reflectors of 8.2 and 5.5 Ma show a wedge-shaped and progradational reflection configuration thickened toward the basin center (Figure 6a and 6b). Through the drilling data from wells DF1529 and LG1120, we distinguished a delta and submarine fan depositional system between reflectors dated at 8.2 and 5.5 Ma in the northernmost part of the central Yingehai-Song Hong Depression (Figure 6). The estimated size of the submarine fan is more than 100 km along both the dip and strike directions. In addition, line 0727 (Figure 4), cutting the strike of line 0738, presents a bidirectional downlapping geometry between the reflectors dated at 8.2 and 5.5 Ma. The seismic facies and sequence stratigraphy identified through the DF1529 core indicate that the delta and submarine fan system was originated from the Red River (Figure 6c).

No clear downlapping structures or progradational reflections indicate that sediments were delivered from Hainan Island. Wells LT1135, YIN2, YIN7, YINQ3 and YX3211 on the eastern shelf penetrated all the Cenozoic sediments and cored sediments of Cretaceous age. Very thin layers of clastic material and carbonate rocks of Plio-Quaternary and mid-Miocene age, respectively, indicate very low sedimentation rates at the shelf. Seismic lines 0727 ad 0735 show aggradation of clinoform started at 5.5 Ma and the clinoform rollover at the eastern margin of the basin did not migrate through time (Figures 4 and 5), which implies that the sediment supply from Hainan Island was stable. In addition, seismic data from the eastern margin display onlapping structures onto the Hainan Uplift, which also suggest limited sediment supply form the Hainan Island. This observation confirms previous zircon and apatite thermochronologic data showing that erosion on Hainan Island after the Oligocene would not be an important source to the Yinggehai-Song Hong basin (Shi et al., 2011).

The most important river draining into the Yinggehai-Song Hong basin from the east coast of Vietnam is the Gianh River, which covers a significantly smaller area (2670 km^2), than that of the Red River catchment (76276 km^2). Limited regional AFT data from bedrock samples from the east coast of Vietnam (Carter et al., 2000) show that the average regional denudation rates is ~34 m/Ma prior to 16 Ma and 390–500 m/Ma between 16-0 Ma (Carter et al., 2000). Assuming a 35% average porosity, the volume of eroded material is estimated as ~0.12×10^3 km^3/Ma (before 16 Ma) and 1.4-1.8×10^3 km^3/Ma (16-0 Ma). The lithology of the east coast of central Vietnam, however, is dominated by carbonates, while the lithology in the center of the basin (as determined primarily from wells) consists of sandy/muddy clastic rocks, not a mixture of carbonates and clastics or carbonate clasts. Therefore, the sediment supply from the east coast of the Vietnam is limited. Core data from DF1529 (Figure 6b) and LG1120 (Figure 2) in the central Yinggehai-Song Hong basin further show that the delta and submarine fan consists predominately of clastic deposits delivered from the longitudinal direction of the Yinggehai-Song Hong basin, which are inferred to derive from the Red River.

5 Stratigraphic Mapping and sediment budget

5.1 Stratigraphic Mapping

Our new high-resolution seismic profiles constrained by detailed nannofossil biostratigraphy from 28 drilling sites allow us to explore the evolution of the sedimentary fill in great detail. As Paleocene-Eocene sequences are not well imaged in the southern part of the central Yinggehai-Song Hong Depression, we focus on the sediment volume since 32 Ma because the high quality seismic reflection data allow us to construct isopach maps.

Figure 7 shows contoured isopach of the major stratigraphic units within the Yinggehai-Song Hong basin. There was no sedimentation on the eastern Slope before 5.5 Ma with the exception of carbonate rocks between 13.8-15.5 Ma. The steepness of the eastern margin of the basin is largely influenced by the Number One fault, especially before 13.8 Ma. Therefore, sedimentation on the eastern side of the basin is closely related to active faulting. In contrast, the western margin of the basin is characterized by gentler slopes generated by several splayed transform faults (Figure 1). In Figure 7, we also show the migration of the depocenter, which was located in the central part of the Central Yinggehai-Song Hong Depression between 23.3–16.5 Ma, and then migrated to the southeastern part of the basin between 16.5 and 13.8 Ma. Between 13.8 and 10.5 Ma, the depocenters moved toward the northwestern sector of the Central Yinggehai-Song Hong Depression. Finally, after 10.5 Ma, the depocenter migrated to the southwestern part of the basin.

5.2 Sediment budget

To compare the volume of sediment in the Yinggehai-Song Hong basin with the eroded material across the onshore Red River drainage area, we estimate the original sediment thickness prior to burial as described in section 3. Average volumes and accumulation rates are calculated for 13 epochs and are summarized in Figure 8. Uncertainties in sediment budget calculations include the effects of post-depositional erosion and uncertainties in compaction estimates, but these errors are moderate and rarely exceed 5%.

The results show a clear pattern of modest sedimentation rates during the Early Miocene (23.3-17.5 Ma), followed by an increase during the period 17.5-12.5 Ma, which is similar to the period 32–23.3 Ma (Figure 8). The Miocene peak at 17.5-12.5 Ma is followed by a sharp drop in the late- Middle Miocene. Relatively steady low depositional rates characterize the period 12.5-5.5 Ma, followed by a three to ten-fold increase in sediment volume rate since the Pliocene time, especially for the period 4.2–3.8 Ma. We discuss the implications of this pattern below.

6 Tectonic subsidence analysis

The tectonic subsidence history of the basin can be calculated by accounting for the loading effects of the sedimentary cover, its burial compaction and the water depth of deposition. We reconstructed the basement subsidence at two deep wells LG1120 and LT11A1 (see locations in Figure 1, and see sediments penetrated by wells in Figures 2 and 4), displaying the thickest stratigraphic columns in the Lingao Uplift and central Yinggehai-Song Hong basin and therefore likely to be representative of the basin as a whole. The subsidence is measured by backstripping the Cenozoic sediments assuming an Airy isostatic basement response and incorporating corrections for compaction and changes in water depth and sea level (Sclater and Christie, 1980; Bond and Kominz, 1984). Because drilling at LG1120 and LT11A1 has demonstrated that the sections were not heavily overpressured, this should be a reasonable approximation of the actual compaction history. The greatest uncertainties in this analysis are in the water depth estimates, although in this region water depth was always less than 200 m. A correction was made for long-term sea-level variations using the reconstruction of Haq et al. (1987). Table 1 shows the starting model for the reconstruction of the basement subsidence curves, showing the different formations and the associated parameters necessary for the calculation.

Figure 9 illustrates the subsidence evolution in the different domains of the Yinggehai-Song Hong basin, which is driven primarily by its tectonic and thermal evolution. The subsidence curves are characterized by marked changes in subsidence rate. The period before 13.8 Ma is characterized by fast subsidence rates of ~84 m My^{-1} and 106 m My^{-1} for wells LG1120 and LT11A1, respectively. The period between 13.8 and 5.5 Ma displays moderate subsidence rates of ~24 m My^{-1}, consistent throughout the entire basin. Finally, the period between 5.5-0 Ma displays a considerable increase in subsidence, which is recorded in different domains of the basin (Figure 9). For example, in the Lingao Uplift a subsidence rate of 145 m My^{-1} is recorded, whereas a subsidence rate of 127 m My^{-1} is observed in the central Yinggehai-Song Hong basin.

7 Stretching and thinning in the Yinggehai-Song Hong basin

In our study we quantify stretching β-factors related to the Paleocene to recent history of the basin and test whether the Cenozoic history of the Yinggehai-Song Hong basin is compatible with a depth-uniform thinning model.

Extension and thinning can be measured at three levels within the continental lithosphere: the upper crust from fault heave analysis, the whole crust from crustal thickness measurements, and the whole lithosphere from subsidence analysis. These techniques have been previously clarified (Davis and Kusznir, 2004; Kusznir and Karner, 2007) and are not described in detail here.

The analysis of upper-crustal faulting to determine Cenozoic upper crustal extension was made from the line 0732 (Figure 2). The seismic data is of high quality and allows the identification of small extensional faults. Fault-derived stretching and thinning factors are shown in Figure 10b. Upper-crustal stretching factors are small, peaking at a stretching factor of 1.26 around the center of the Yinggehai-Song Hong basin.

The crustal structure of the line 0793 is derived from Gong et al. (1997) taken from an inversion of Bouguer gravity anomaly data. The crustal stretching is calculated assuming an initial homogenous pre-rift crustal thickness of 32 km (Jin and Sun, 1997). Figure 10f shows the profiles of crustal thinning-derived stretching factors. The peak value is 2.3 in the central part of the seismic line.

Flexural backstripping, decompaction and reverse post-breakup thermal subsidence modeling has been carried out on the line 0793 to determine a lithospheric stretching factor. Compaction parameters from Sclater and Christie (1980) have been used. The assumption that the unconformities dated at 23.3 Ma at the Lingao Uplift and Eastern Slope were at (or near) sea level has been used as a palaeobathymetric constraint for the flexural backstripping (Figure 10d). While a range of values of the effective elastic thickness of the plate Te (0, 3, 5, 10 and 25 km) was used in the flexural backstripping, these results are relatively insensitive to this parameter, because the wavelength associated with loading is long. The resulting stretching factor profile for the Cenozoic lithosphere stretching event is shown in Figure 10e, assuming Te=3 km, which is same as previous work (Clift, et al., 2002). The result shows a value of 4 in the central part of the profile decreasing toward 1 in the east and 3 in the west.

Upper-crustal, whole-crustal and lithospheric stretching factors for the Yinggehai-Song Hong basin are summarized in Figure 10f. The summed extension observed in the upper crust is substantially less than that observed for the whole crust or whole lithosphere, which suggests depth-dependent stretching of the continental lithosphere.

8. Discussion

8.1 River basin organization in the SE Asia

The modern Yinggehai-Song Hong basin has three potential source areas: the Red River catchment, Hainan Island and Vietnam coast. However, low temperature thermochronometric data imply no large sediment supply from the Hainan Island (Shi et al., 2011) since the Miocene and east coast of the Vietnam since the Oligocene (Carter et al., 2000). We reinforce these conclusions through our data; no clear downlapping structures younger than 5.5 Ma from the Hainan Island and Vietnam coast can be identified from our new high-resolution seismic profiles, which densely cover the whole basin. In contrast, on the northern side of the basin the unit shows well developed steeply dipping clinoforms prograding towards the southeast. Downlapping relationship with the lower unit suggests a dominant sediment influx from the Red River drainage. The large scale Red

River delta/submarine fan depositional system depicted in Figure 6 demonstrates the large sediment budget of the Red River, which rapidly accumulated along the axial direction of the Yingehai-Song Hong basin.

One would expect significant changes in the sedimentation rate to occur if rock uplift and precipitation are the key controls on erosion, or if major headwater capture has occurred within the paleo-Red River catchment. We have shown that accumulation rates were low during 23.3-17.5 and 12.5-5.5 Ma and fast during 32-23.3 Ma, 17.5–12.5 Ma and 5.5-0 Ma (Figure 8). It has been suggested that sedimentation rates, which are genetically correlated with erosion in the source area, increased globally since 5.5 Ma, consistent with the hypothesis that Pliocene-Pleistocene climate change enhanced global erosion (Hay et al., 1988; Métivier et al., 1999; Willett, 2010; Zhang et al., 2001). Our study identified two peaks in sedimentation rate at 4.2–3.8 and 2.4-1.9 Ma since the Pliocene. The peak sediment accumulation rates are roughly 3–5 times those during the periods 3.8–2.4 and 1.9-0 Ma, and are considerably higher than those inferred for the preceding tens of million years. In the southeastern margin of Tibetan Plateau (e.g. Yunan and northern Vietnam) thermochronometric studies of detrital minerals indicate an acceleration in exhumation and erosion after ca. 4 Ma (Schoenbohm et al., 2006), which correlates with strengthening and rapid fluctuations of the monsoon in Asia since that time (Clift et al., 2008). Therefore we attribute the increase of sedimentation since 5.5 Ma in the basin to the rapid climate variability since the Pliocene.

Strike-slip motion along the Red River fault zone strongly affected the geology and topography of the eastern Tibetean plateau margin and must have been instrumental in helping to guide the reorganization of rivers in the region. Dating of the onshore Red River

Fault Zone shows that sinistral motion started ca. 34 Ma and was most rapid after 27 Ma and before 17 Ma (Gilley et al., 2003; Leloup et al., 2001) with widely varying estimates of total slip of 500-1400 km (Harrison et al., 1992; Leloup et al., 2001; Tapponnier et al., 1990). However, the seismic data in our seismic data library show strong activity of the offshore Red River fault before 13.8 Ma, that is 3-4 Ma after the major faulting of the onshore Red River fault (Leloup et al., 2001), and quiescence since 5.5 Ma. If strike-slip faulting is the cause of the river capture, river capture would not occur later than 17 Ma, after cessation of the left lateral strike-slip motion related to the progressive growth of Tibetan topography toward the southeast.

The headwater capture from the Paleo-Red River must result in an abrupt reduction of the sediment accumulation rate in the Yinggehai-Song Hong basin. Our study presents significantly lower sediment accumulation rates between 23.3-17.5 and 12.5-5.5 Ma, which could indeed reflect a loss of drainage area. However, this timing does not match well the slow exhumation during the Middle to Late Miocene inferred from thermochronometry (Harrison et al., 1996). This decrease in sediment supply from Red River drainage is also synchronous with increased aridity and stronger winter monsoon across Asia (Derry and France-Lanord, 1996; Dettman et al., 2003; Gupta et al., 2004; Wan et al., 2009). The timing of the decrease in sedimentation rate matches more closely this change in climatic forcing.

According to Wan et al. (2012), there were strong summer monsoons between 22 and 17 Ma. This should result in higher sedimentation rates in the Yinggehai-Song Hong basin. However, we observe the opposite in our calculated sediment budget (Figure 8). A possible explanation for this discrepancy is that sediment flux was affected by capture of the Red

River during the Early Miocene (23.3–17.5 Ma) as a consequence of heavy monsoon erosion, which would have diverted any sediment pulse from eastern Tibet and SW China into the East China Sea.

8.2 Fast basin subsidence and lower crustal/mantle flow

Our analyses show that the basin exhibited fast subsidence rates after 5.5 Ma. Since our high-resolution seismic reflection data do not support deformation along the Red River fault in the basin within the last 5.5 Ma, we judge unlikely fast subsidence related to strike-slip deformation as suggested by Xie and Heller (2009). Other sources of subsidence during the last 5.5 Ma may be related to lower crustal and mantle flow. For example, previous works have proposed that, in regions of high heat flux, less viscous lower crust may flow to equilibrate lateral pressure gradients (Block and Royden, 1990; Bird, 1991; Wdowinski and Axen, 1992). This process may result in crustal thinning, as observed across rifted continental margins (e.g. Davis and Kusznir et al.; Liao et al., 2011).

Models in which the lower crust and mantle motion provide a substantial contribution to the surface evolution of the sedimentary basin, are also consistent with our estimates of the β-factors related to crustal and lithospheric stretching. The Yinggehai-Song Hong basin experienced only limited upper-crustal extension ($\beta \leqslant 1.26$), yet the Red River catchments delivered 12 km of post-rift sequences (23.3-0 Ma), of which 3-4 km were emplaced since 5.5 Ma. Conventional post-rift backstripping would require uniform lithospheric thinning by stretching factor larger than 100 to explain these tremendous thicknesses, which indicates an oceanic stretching factor. However, the Yinggehai-Song Hong basin is not thought to be floored by oceanic crust. Therefore, we think the basin must be floored by anomaly crust of extreme thinned crust, possibly exhumed mantle. This is similar with the sediments locally overlaid on the exhumed mantle in the Phu Khanh Basin in the SW margin of the South China Sea (Savva et al.2013), whose extension rate is also very large. Thus our results suggest that some mantle and lower crust flow contributed significantly more than the upper crustal thinning to the surface evolution since the Cenozoic. This implies that the depth-uniform thinning model of basin formation (McKenzie, 1978) is not applicable to the Cenozoic history of the Yinggehai-Song Hong basin, while a depth-dependent lithosphere-scale thinning may be more appropriate, which is also observed in its neighbor, Qiongdongnan (Lei et al., 2013). Seismic tomography shows that the crust at 15 km depth beneath the Yinggehai-Song Hong basin has low (up to 2% below average) seismic velocities (Lei et al., 2009), indicating relatively high temperatures. This is supported by petroleum exploration wells, which show that the geothermal gradient in the Yinggehai-Song Hong basin is high (i.e., 46°C/km) (Hao et al., 1995). Therefore, we postulate that fast subsidence of the Yinggehai-Song Hong basin after 5.5 Ma may arise from the occurrence of lithospheric warming, weakening and thinning by lower crustal and/or mantle flow resulting from collision between India-Eurasia and Indian oceanic subduction below the Eurasia.

9. Conclusions

In this study we explored the onshore tectonics and river organization of SE Asia from the observed offshore stratigraphy in the Yinggehai-Song Hong basin during the Cenozoic period. A new grid of high-resolution seismic profiles tied to wells with biostratigraphic age control allowed us to examine the changes in sediment delivery rate from the Red

River, which is related to both tectonics and climate in SE Asia. Our analysis showed that the sedimentary section comprises a thick Cenozoic sequence, which is affected strongly by faulting of the offshore Red River fault and basement subsidence of the basin. Most of the offshore Red River fault terminated at an unconformity dated at 13.8 Ma. The result of the sediment accumulation rates shows several prominent shifts, including a sharp decrease at 23.3 Ma and 12.5 Ma respectively, and a sharp increase at 5.5 Ma. The sediment decompaction calculations show sharply reduced sedimentation rate at 12-13 Ma, which match similar trends in South Asia and the Pearl River Mouth basin as result form monsoon weakened at that time. Fast sedimentation resumed in the last 5.5 Ma, which is likely the consequence of the onset of cyclical glacial-interglacial climate during the Plio-Pleistocene and is part of a global change in erosion at that time. Reconstructions show that sediment flux to the Yinggehai-Song Hong basin changed markedly from the Oligocene and early Miocene. However, because the Asian monsoon begins to strengthen significantly in the early Miocene (Wan et al., 2012), the loss of drainage area might have been offset by the increased sediment flux driven by the more erosive climate. We favor major headwater capture away from the Red River to predate the Middle Miocene, probably during the Oligocene and early Miocene.

We have shown that the Yinggehai- Song Hong basin has experienced an apparently anomalous fast subsidence history since the Pliocene-Quaternary. Qualifying stretching and thinning of the basin indicates the Cenozoic history of the Yinggehai-Song Hong basin is compatible with a depth-dependent lithospheric thinning model. We suggest that a combination of the mantle and lower crustal flow originated by collision between India-Eurasia and Indian oceanic subduction below the Eurasia may explain the large subsidence since the Pliocene-Quaternary, but paucity of faulting.

Acknowledgements

Our first acknowledgments go to the editor and the five reviewers for constructive criticism that helped considerably to improve this article. We are grateful to Weilin Zhu from CNOOC, who kindly provided us with the seismic and well data used in this work. We also acknowledge grants from Natural Science Foundation of China (No. 91028009，41302082, 41272121), the Programme of Introducing Talents of Discipline to Universities (No. B14031) and the foundation of State Key Laboratory of Petroleum Resources and Prospecting, China University of Petroleum, Beijing (No.PRP/open-1404). Map of region around Yinggehai-Song Hong basin is generated by GeoMapApp. Alan Roberts is thanked for allowing use of Flex-Decomp™ to study subsidence history. Chao Lei thanks the China Scholarship Council for supporting his study at Earth Surface Dynamics group of ETH Zurich.

References:

Allen, C.R. et al., 1984. Red River and associated faults, Yunnan Province, China: Quaternary geology, slip rates, and seismic hazard. Bulletin of the Geological Society of America, 95(6): 686-700.

An, Z., Kutzbach, J.E., Prell, W.L. and Porter, S.C., 2001. Evolution of Asian monsoons and phased uplift of the Himalaya-Tibetan plateau since Late Miocene times. Nature, 411(6833): 62-66.

Athy, L.F., 1930. Density, porosity, and compaction of sedimentary rocks. AAPG Bulletin 14(1): 1-24.

Bahr, D. B., Hutton, E. W. H., Syvitski, J. P. M., and Pratson, L. F., 2001, Exponential approximations to compacted sediment porosity profiles: Computers & Geosciences, 27(6):691-700.
Bond, G. C., and Kominz, M. A., 1984, Construction of tectonic subsidence curves for the early Paleozoic miogeocline, southern Canadian Rocky Mountains: Implications for subsidence mechanisms, age of breakup, and crustal thinning: Geological Society of America Bulletin, 95(2): 155-173.
Brookfield, M.E., 1998. The evolution of the great river systems of southern Asia during the Cenozoic India-Asia collision: rivers draining southwards. Geomorphology, 22(3-4): 285-312.
Bird, P., 1991. Lateral extrusion of lower crust from under high topography in the isostatic limit. Journal of Geophysical Research: Solid Earth (1978–2012) 96, 10275-10286.
Carter, A., Roques, D., Bristow, C.S., 2000. Denudation history of onshore central Vietnam: constraints on the Cenozoic evolution of the western margin of the South China Sea. Tectonophysics 322, 265-277.
Clark, M.K. et al., 2004. Surface uplift, tectonics, and erosion of eastern Tibet from large-scale drainage patterns. Tectonics, 23(1): 1006-1029.
Clift, P., Lin, J., Barckhausen, U., 2002. Evidence of low flexural rigidity and low viscosity lower continental crust during continental break-up in the South China Sea. Marine and Petroleum Geology 19, 951-970.
Clift, P. and Sun, Z., 2006. The sedimentary and tectonic evolution of the Yinggehai–Song Hong basin and the southern Hainan margin, South China Sea: Implications for Tibetan uplift and monsoon intensification. Journal of Geophysical Research: Solid Earth. 111.
Clift, P. Hodges K., Heslop D., Hannigan R., Hoang V. and Calves G. 2008. Correlation of Himalayan exhumation rates and Asian monsoon intensity. Nature Geoscience, 1(12): 875-880.
Clift, P., Blusztajn, J. and Duc, N.A., 2006. Large-scale drainage capture and surface uplift in eastern Tibet-SW China before 24 Ma inferred from sediments of the Hanoi Basin, Vietnam. Geophysical Research Letters, 33: L19403.
Davis, M. and Kusznir, N.J. 2004. Depth-dependent lithospheric stretching at rifted continental margins. In: Karner, G.D. (ed.) Proceedings of NSF Rifted Margins Theoretical Institute. Columbia University Press, 92–136.
Derry, L.A. and France-Lanord, C., 1996. Neogene Himalayan weathering history and river 87Sr/86Sr: impact on the marine Sr record. Earth and Planetary Science Letters, 142(1-2): 59-74.
Dettman, D.L., Fang, X., Garzione, C.N. and Li, J., 2003. Uplift-driven climate change at 12 Ma: a long $\delta^{18}O$ record from the NE margin of the Tibetan plateau. Earth and Planetary Science Letters, 214(1-2): 267-277.
Fournier, M., Jolivet, L., Davy, P., Thomas, J., 2004. Backarc extension and collision: an experimental approach to the tectonics of Asia. Geophysical Journal International. 157 (2), 871–889.
Gilley, L.D., Harrison, T.M., Leloup, P.H., Ryerson, F.J., Lovera, O.M., Wang, J.H., 2003. Direct dating of left-lateral deformation along the Red River shear zone, China and Vietnam. Journal of Geophysical Research: Solid Earth, 108.

Gong, Z. and Li, S., 1997. Continental Margin Basin Analysis and Hydrocarbon Accumulation of the Northern South China Sea. Science Press, Beijing.

Gupta, A.K., Singh, R.K., Joseph, S., and Thomas, E., 2004. Indian Ocean high-productivity event (10–8 Ma): linked to global cooling or to the initiation of the Indian monsoons? Geology, 32(9): 753–756.

Hao, F., Sun, Y., Li, S. and Zhang, Q., 1995. Overpressure retardation of organic-matter maturation and petroleum generation: a case study from the Yinggehai and Qiongdongnan Basins, South China Sea. American Association of Petroleum Geologists Bulletin, 79(4): 551-562.

Haq, B.U., Hardenbol, J. and Vail, P.R., 1987. Chronology of fluctuating sea levels since the Triassic. Science, 235(4793): 1156.

Harrison, T. M., Leloup, P. H., Ryerson, F. J., Tapponnier, P., Lacassin, R., and Chen, W.,1996. Diachronous initiation of transtension along the Ailao Shan-Red River shear zone, Yunnan and Vietnam. In: Yin A. and Harrison T. M. (ed.) The Tectonic Evolution of Asia, Cambridge Univ. Press, New York, 208 – 226,

Hay, W.W., Sloan, J.L.I. and Wold, C.N., 1988. Mass/Age Distribution and Composition of Sediments on the Ocean Floor and the Global Rate of Sediment Subduction. Journal of Geophysical Research, 93(B12): 14933-14940.

Van Hoang, L., Clift, P.D., Schwab, A.M., Huuse, M., Nguyen, D.A., Zhen, S., 2010. Large-scale erosional response of SE Asia to monsoon evolution reconstructed from sedimentary records of the Song Hong-Yinggehai and Qiongdongnan basins, South China Sea. Geological Society, London, Special Publications 342, 219-244.

Jolivet, L., Tamaki, K., Fournier, M., 1994. Japan Sea, opening history and mechanism: A synthesis. Journal of Geophysical Research: Solid Earth 99, 22237-22259.

Jolivet, L., Maluski, H., Beyssac, O., Goff,, B., Lepvrier, C., Thi, P.T., Vuong, N.V., 1999. Oligocene-Miocene Bu Khang extensional gneiss dome in Vietnam: Geodynamic implications. Geology 27 (1), 67-70.

Jin W S, Sun D Z. ,1997. Deep crust structure and its evolution of South China continent . Beijing: Geological Publishing House.

Kong, P., Zheng, Y. and Caffee, M.W., 2012. Provenance and time constraints on the formation of the first bend of the Yangtze River. Geochem. Geophys. Geosyst., 13: Q06017.

Kusznir, N. J. and Karner, G. D., 2007. Continental lithospheric thinning and breakup in response to upwelling divergent mantle flow: application to the woodlark, Newfoundland and Iberia margins. In Karner G. D., Manatschal G. and Pinheiro L. M. (ed.) Imaging, Mapping and Modelling Continental Lithosphere Extension and Breakup. Geological Society, Special Publications, 282, 389-419

Leech, M.L., Singh, S., Jain, A.K., Klemperer, S.L. and Manickavasagam, R.M., 2005. The onset of India-Asia continental collision: Early, steep subduction required by the timing of UHP metamorphism in the western Himalaya. Earth and Planetary Science Letters, 234(1-2): 83-97.

Lei, C., Ren, J., Clift, P., Wang, Z., Li, X., Tong, C, 2011. The structure and formation of diapirs in the Yinggehai-Song Hong Basin, South China Sea. Marine and Petroleum Geology, 28: 980-991.

Lei, C., Ren, J., Tong, D., 2013. Geodynamics of the ocean-continent transition zone, northern margin of the South China Sea: implications for the opening of the South China Sea. Chinese Journal of Geophysics-Chinese Edition 56, 1287-1299.

Lei, J., Zhao, D, Steinberger, B. Wu, B., Shen, F., Li, ., 2009. New seismic constraints on the upper mantle structure of the Hainan plume. Physics of the Earth and Planetary Interiors, 173(1-2): 33-50.

Leloup, P.H., Arnaud, N., Lacassin, R., Kienast, J.R., Harrison, T.M., Trong, T.T., Replumaz, A., Tapponnier, P., 2001. New constraints on the structure, thermochronology, and timing of the Ailao Shan-Red River shear zone, SE Asia. Journal of Geophysical Research, 106(B4): 6683-6732.

Leloup, P.H., Lacassin, R., Tapponnier, P. and Schärer, U., 1995. The Ailao Shan-Red River shear zone (Yunnan, China), Tertiary transform boundary of Indochina. Tectonophysics, 251(1-4): 3-10.

Liao, J., Zhou, D., Zhao, Z., Zhang, Y. and Xu, Z., 2011. Numerical modeling of the anomalous post-rift subsidence in the Baiyun Sag, Pearl River Mouth Basin. Science China Earth Sciences, 54(8): 1156-1167.

McKenzie, D., 1978. Some remarks on the development of sedimentary basins. Earth and Planetary Science Letters, 40(1): 25-32.

Métivier, F., Gaudemer, Y., Tapponnier, P. and Klein, M., 1999. Mass accumulation rates in Asia during the Cenozoic. Geophysical Journal International, 137(2): 280-318.

Molnar, P. and Tapponnier, P., 1975. Cenozoic tectonics of Asia: effects of a continental collision. Science, 189(4201): 419-426.

Molnar, P., England, P. and Martinod, J., 1993. Mantle dynamics, uplift of the Tibetan Plateau, and the Indian monsoon. Reviews of Geophysics, 31(4): 357-396.

Peltzer, G. and Tapponnier, P., 1988. Formation and evolution of strike-slip faults, rifts, and basins during the India-Asia collision: An experimental approach. Journal of Geophysical Research, 93(B12): 15085-15,117.

Rangin, C., Klein, M., Roques, D. and Le Pichon, X., 1995. The Red River fault system in the Tonkin Gulf, Vietnam. Tectonophysics, 243(3-4): 209-222.

Replumaz, A., Lacassin, R., Tapponnier, P., Leloup, P.H., 2001. Large river offsets and Plio-Quaternary dextral slip rate on the Red River fault (Yunnan, China). Journal of Geophysical Research: Solid Earth, 106, 819-836.

Replumaz, A., Guillot, S., Villaseñor, A., Negredo, A.M., 2013. Amount of Asian lithospheric mantle subducted during the India/Asia collision. Gondwana Research 24, 936-945.

Richardson, N.J., Densmore, A.L., Seward, D., Wipf, M. and Yong, L., 2010. Did incision of the Three Gorges begin in the Eocene? Geology, 38 (6): 551-554.

Royden, L., 1997. Surface deformation and lower crustal flow in Eastern Tibet. Science, 276.

Sangree, J.B. and Widmier, J.M., 1979. Interpretation of depositional facies from seismic data. Geophysics, 44(2): 131-160.
Schoenbohm, L.M., Burchfiel, B.C. and Liangzhong, C., 2006. Propagation of surface uplift, lower crustal flow, and Cenozoic tectonics of the southeast margin of the Tibetan Plateau. Geology, 34(10): 813-816.
Sclater, J.G. and Christie, P., 1980. Continental stretching: an explanation of the post-mid-Cretaceous subsidence of the central North Sea basin. Journal of Geophysical Research, 85(B7): 3711-3739.
Searle, M.P., Yeh, M., Lin, T. and Chung, S., 2010. Structural constraints on the timing of left-lateral shear along the Red River shear zone in the Ailao Shan and Diancang Shan Ranges, Yunnan, SW China. Geosphere, 6 (4): 316-338.
Shi, X., Kohn, B., Spencer, S., Guo, X., Li, Y., Yang, X., Shi, H., Gleadow, A., 2011. Cenozoic denudation history of southern Hainan Island, South China Sea: Constraints from low temperature thermochronology. Tectonophysics 504, 100-115.
Sun, Z., Zhou, D., Zhong, Z., Zeng, Z. and Wu, S., 2003. Experimental evidence for the dynamics of the formation of the Yinggehai basin, NW South China Sea. Tectonophysics, 372(1-2): 41-58.
Sternai, P., Jolivet, L., Menant, A., Gerya, T., 2014. Driving the upper plate surface deformation by slab rollback and mantle flow. Earth and Planetary Science Letters, 405, 110-118.
Tapponnier, P., Lacassin, R., Leloup, P.H., Schärer, U., Dalai, Z., Haiwei, W., Xiaohan, L., Shaocheng, J., Lianshang, Z., Jiayou, Z., 1990. The Ailao Shan/Red River metamorphic belt: Tertiary left-lateral shear between Indochina and South China. Nature 343, 431-437.
Tapponnier, P., Zhiqin, X., Roger, F., Meyer, B., Arnaud, N., Wittlinger, G., Jingsui, Y., 2001. Oblique stepwise rise and growth of the Tibet Plateau. science 294, 1671-1677.
Taylor, B., Hayes, D.E., 1983. Origin and history of the South China Sea basin. The Tectonic and Geologic Evolution of Southeast Asian Seas and Islands: Part 2, 23-56.
Taylor, B. and Hayes, D. E., 1983. Origin and History of the South China Sea Basin. In Hayes D. E. (ed.)The Tectonic and Geologic Evolution of Southeast Asian Seas and Islands: Part 2, American Geophysical Union, Washington, D. C..
Walker, J.D. and Geissman, J.W., 2009. Geologic time scale. Geological Society of America.
Wan, S.M., Kurschner, W.M., Clift, P.D., Li, A.C. and Li, T.G., 2009. Extreme weathering/erosion during the Miocene Climatic Optimum: Evidence from sediment record in the South China Sea. Geophysical Research Letters, 36: L19706.
Wang, Y., Xu, Q., Li, D., Han, J., Lü, M., Wang, Y., Li, W., Wang, H., 2011. Late miocene red river submarine fan, northwestern South China Sea. Chinese Science Bulletin 56, 1488-1494.
Willett, S.D., 2010. Late Neogene Erosion of the Alps: A Climate Driver? Annual Review of Earth and Planetary Sciences, 38: 411-437.

Wdowinski, S., and G. J. Axen, 1992, Isostatic rebound due to tectonic denudation: A viscous flow model of a layered lithosphere, Tectonics, 11(2), 303–315

Xie, X. and Heller, P.L., 2009. Plate tectonics and basin subsidence history. Geological Society of America Bulletin, 121: 55-64.

Zachos, J., Pagani, M., Sloan, L., Thomas, E. and Billups, K., 2001. Trends, rhythms, and aberrations in global climate 65 Ma to present. Science, 292(5517): 686-693.

Zhang, P., Molnar, P. and Downs, W.R., 2001. Increased sedimentation rates and grain sizes 2-4 Myr ago due to the influence of climate change on erosion rates. Nature, 410(6831): 891-897.

Zheng, H., Clift, P.D., Wang, P., Tada, R., Jia, J., He, M., Jourdan, F., 2013. Pre-Miocene birth of the Yangtze River. Proceedings of the National Academy of Sciences 110, 7556-7561.

Zhu, M., Graham, S. and McHargue, T., 2009. The Red River Fault zone in the Yinggehai Basin, South China Sea. Tectonophysics, 476(3-4): 397-417.

Zhu, W. and Lei, C., 2013. Refining the model of South China Sea's tectonic evolution: evidence from Yinggehai-Song Hong and Qiongdongnan Basins. Marine Geophysical Research, 34(3): 325-339.

figures and table

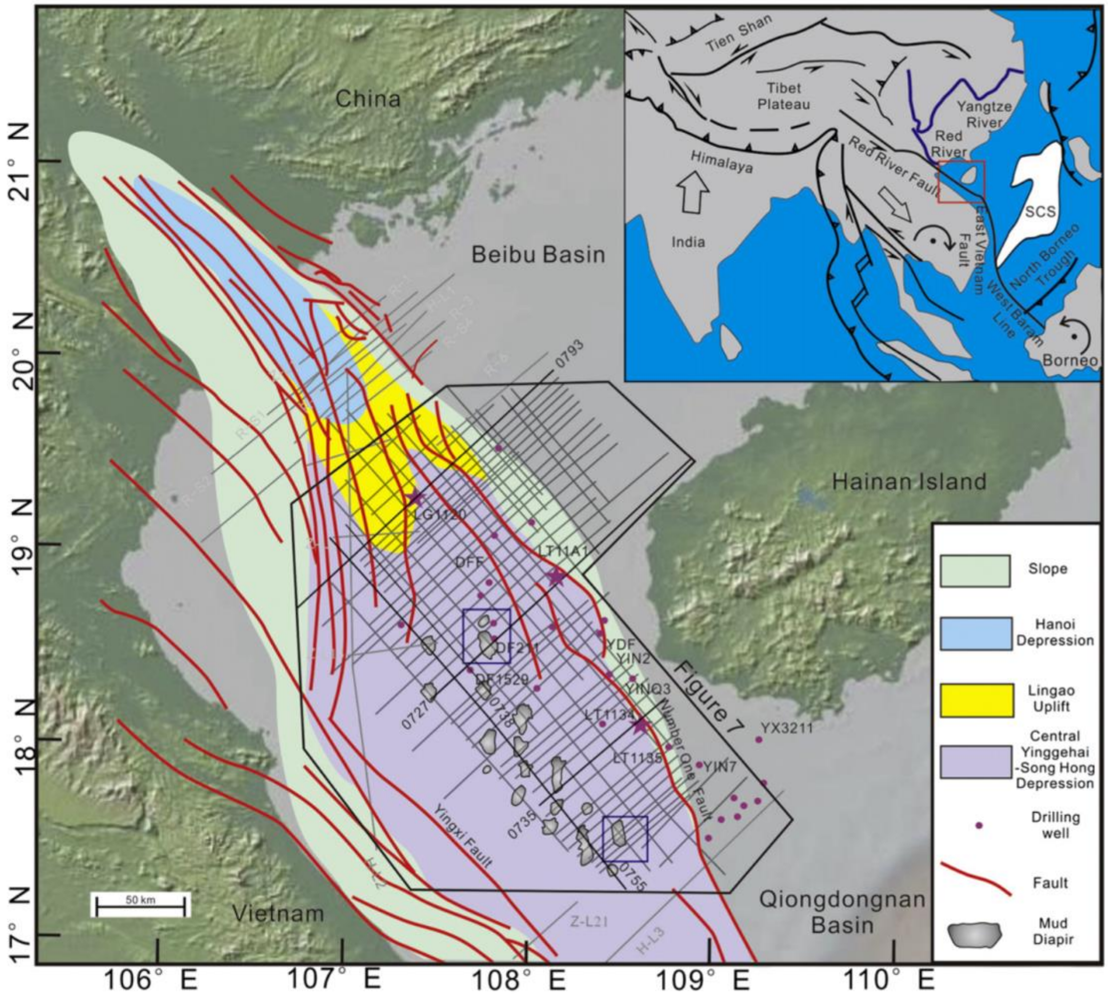

Fig. 1 Location map for the study area, showing the total seismic reflection data set considered and drilling wells (brown stars and solid points). The seismic lines marked by R, Z and H adopted from Rangin et al (1995), Zhu et al (2009) and Van Hoang et al (2010), and the others (black solid and grey solid lines) are from our available seismic profiles library. Blue boxes outline the extent of the 3D seismic data used in this study. Diapirs are modified after Lei et al (2011). The Red box and blue solid lines in the inset map of tectonics and geology of Southeast Asia shows location of Yinggehai-Song Hong basin and rivers discussed in this paper. SCS: South China Sea, YDF: Yingdong fault, DFF: Dongfang fault, YXF: Yingxi fault.

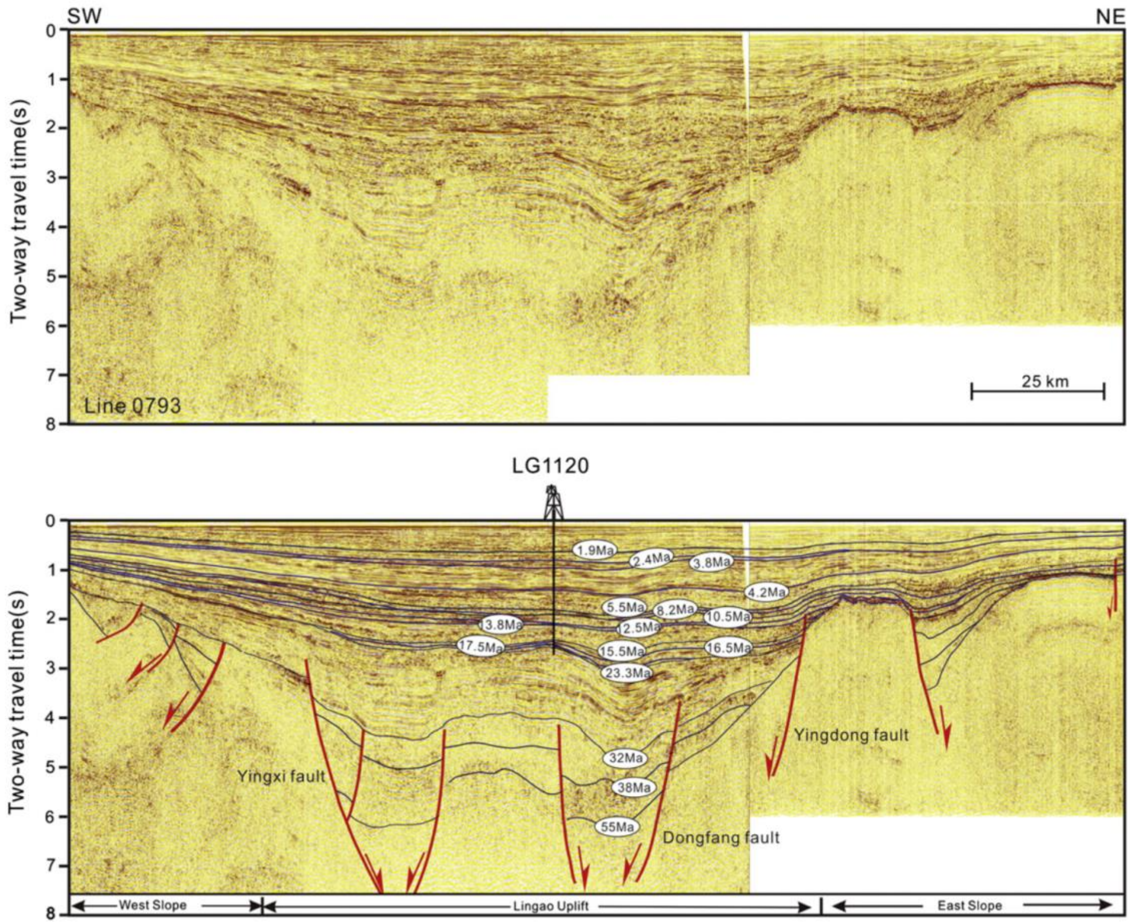

Fig.2 Uninterpreted and interpreted regional seismic section of line 0793 running from southwest to northeast through the Yinggehai-Song Hong basin. Basement is characterized by strong faulting, which formed a succession of graben-horst structures. Line location is shown on Figure 1.

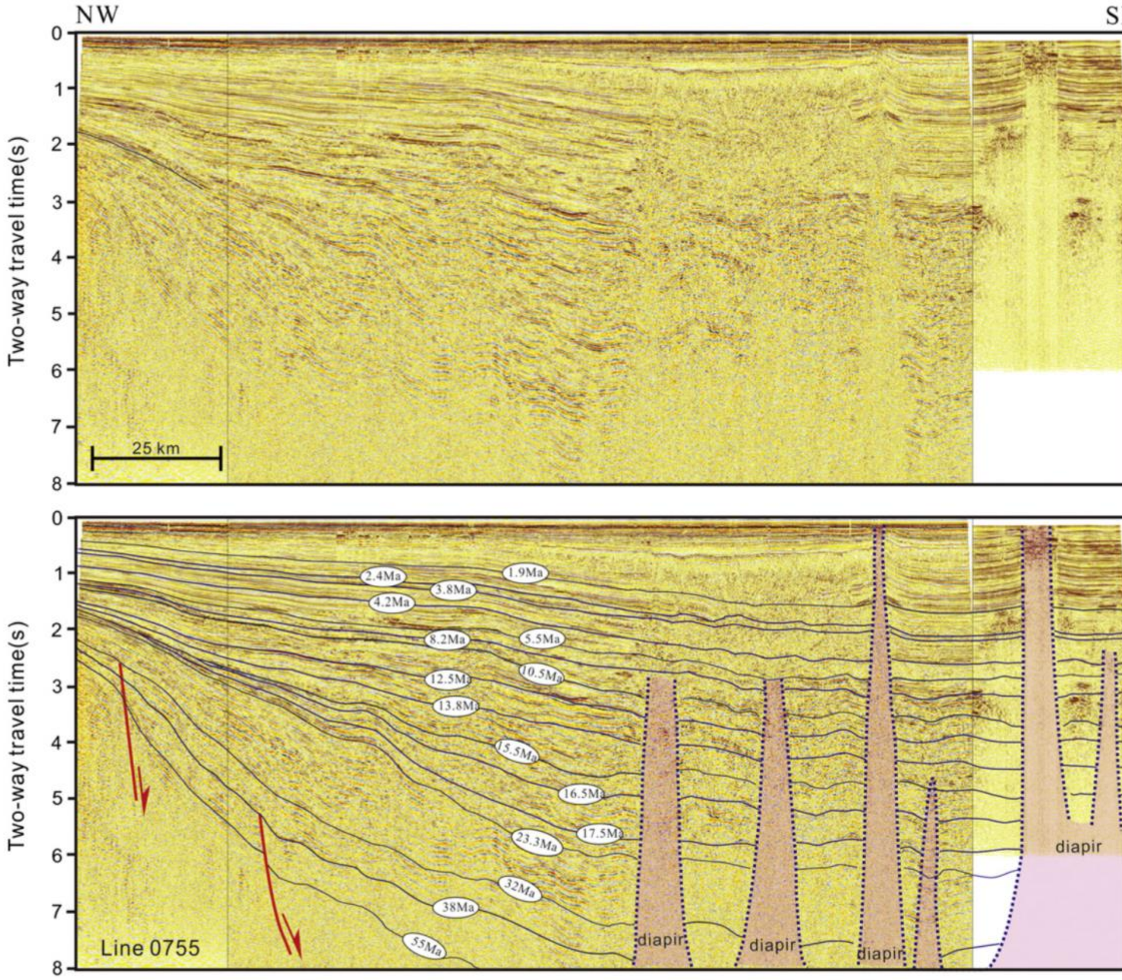

Fig.3 Interpreted regional seismic section of line 0755 from the northwest to southeast through the Yinggehai-Song Hong basin. The progradation configuration since the 23.3 Ma observed here suggests sediments spilled over to the Southeast. A large volume of sediment was trapped in the center of the basin and several pronounced large-scale shale diapirs appear there. Line location is shown on Figure 1.

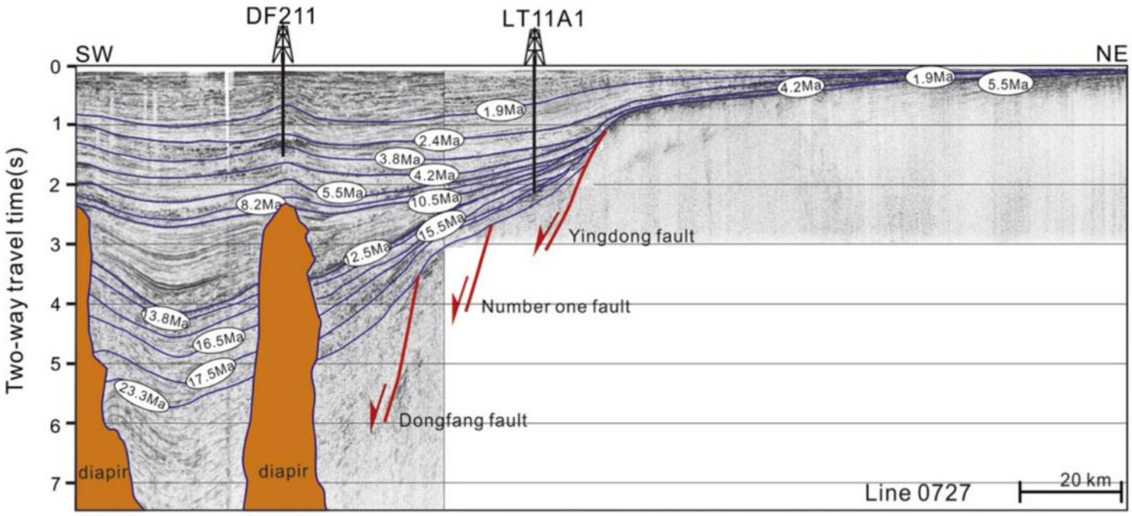

Fig.4 Interpreted seismic section of line 0727 from the eastern margin of the Yinggehai-Song Hong basin. Line location is shown on Figure 1.

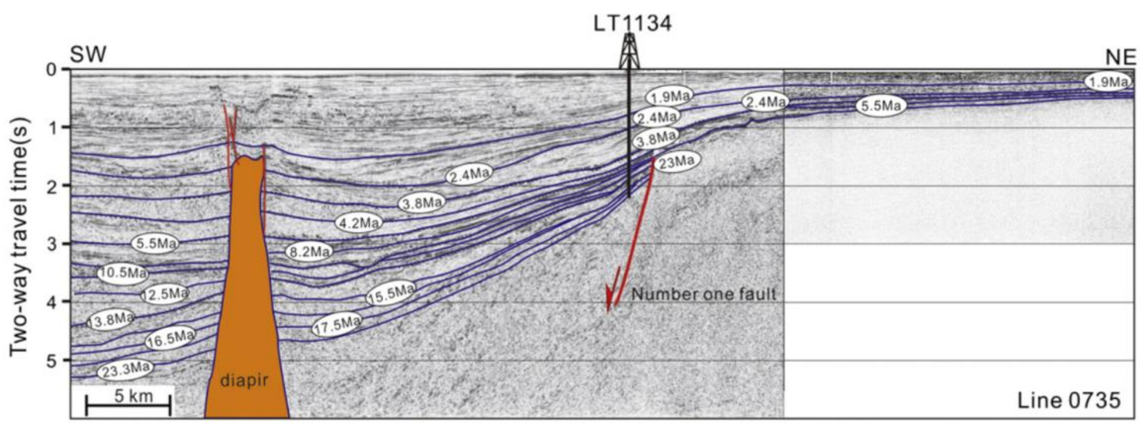

Fig.5 Interpreted seismic section of line 0735 running the eastern margin of the Yinggehai-Song Hong basin. The seismic section shows diaprism and increased sediments thickness toward the Central Yinggehai Depression. Line location is shown on Figure 1.

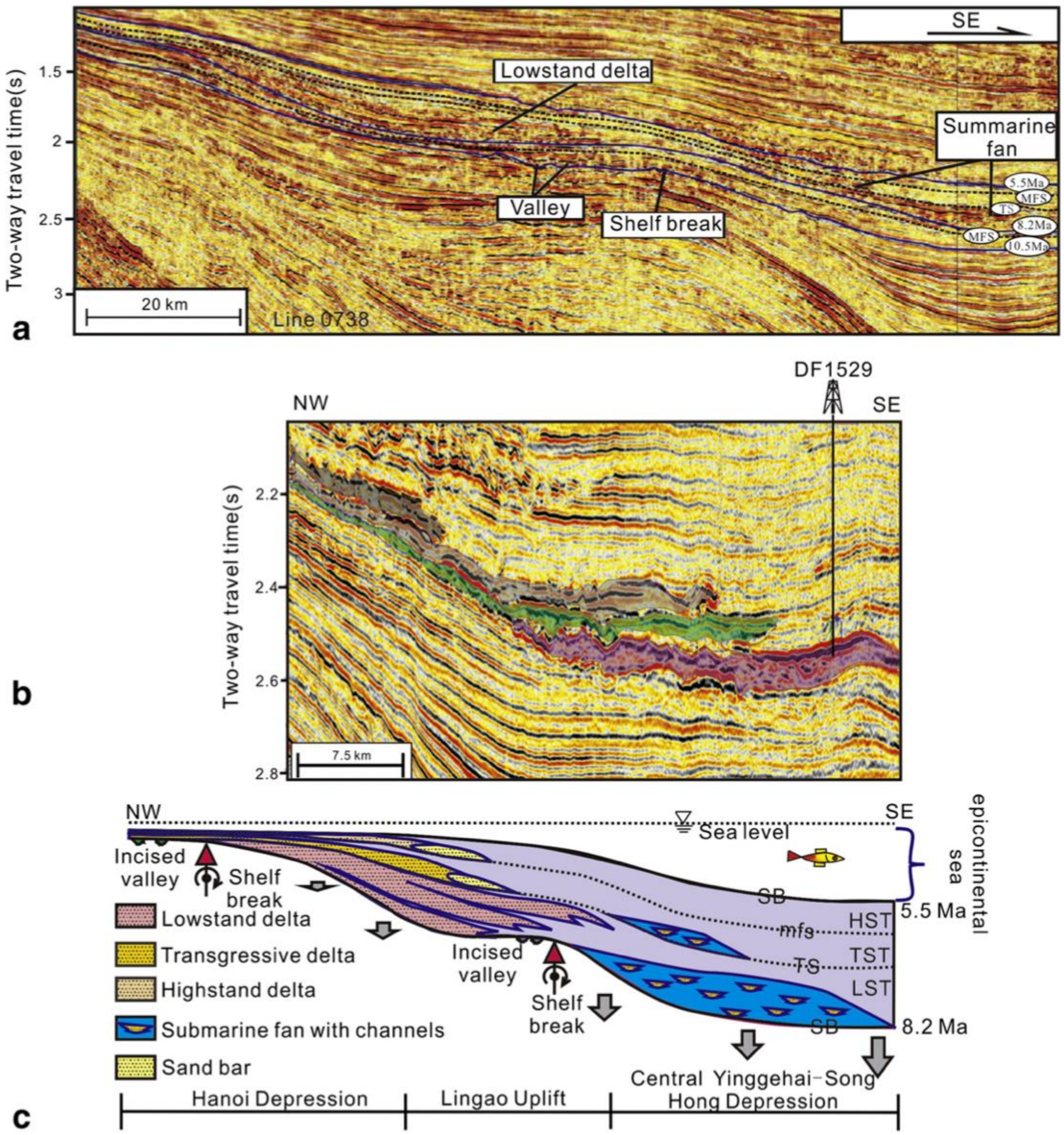
SE
Lowstand delta
Summarine fan
Valley
Shelf break
5.5Ma
MFS
TS
8.2Ma
MFS
10.5Ma
Two-way travel time(s)
20 km
Line 0738
a
DF1529
NW
SE
Two-way travel time(s)
7.5 km
b
NW
SE
Sea level
epicontinental sea
Incised valley
Shelf break
SB
5.5 Ma
HST
mfs
TST
TS
LST
8.2 Ma
SB
Lowstand delta
Transgressive delta
Highstand delta
Submarine fan with channels
Sand bar
Incised valley
Shelf break
Hanoi Depression
Lingao Uplift
Central Yinggehai–Song Hong Depression
c

752

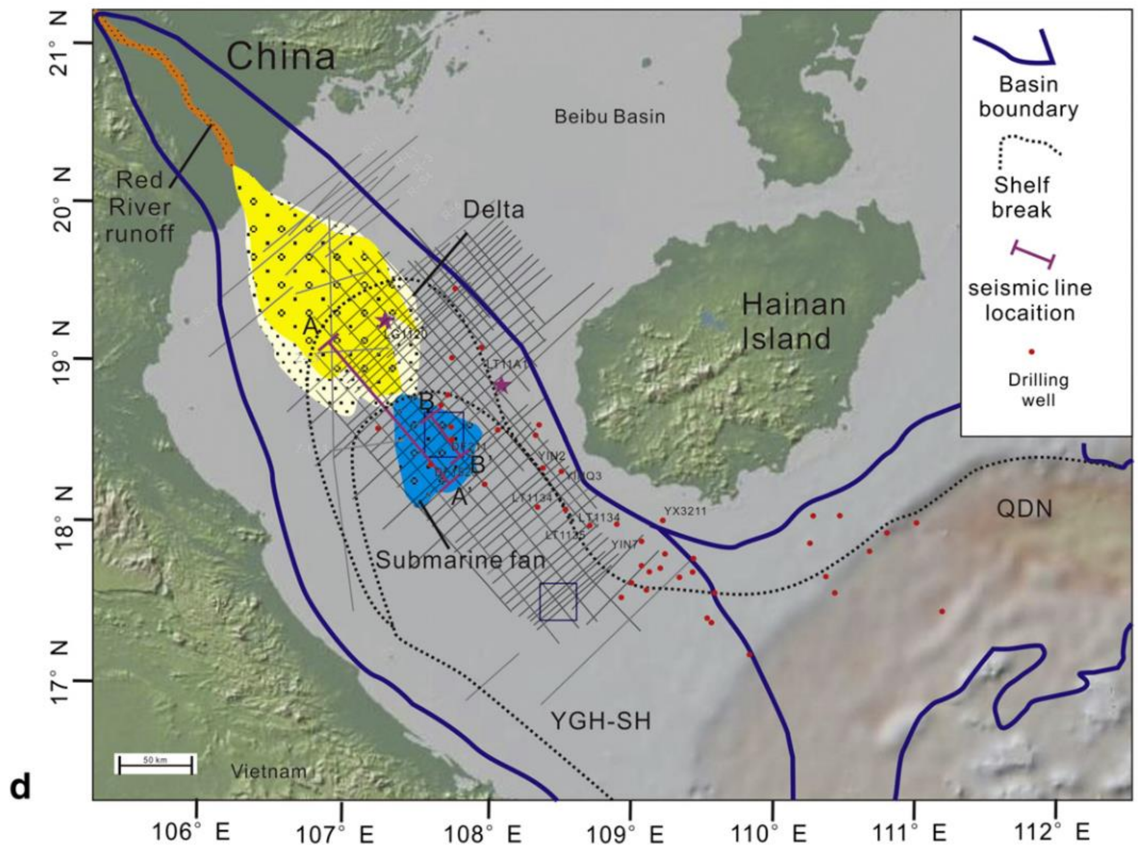

Fig.6 (a) 2D Seismic profile, Line 0738, along the strike of the Red River system dispersion in Miocene time shows characteristics of a submarine fan.; (b) a better resolution of seismic profile from 3D seismic data shows a close-up of the investigated submarine fan constrained by the well DF1529 that allows its evolution to be seen more clearly. (c) Conceptual sketch of the Red River delta and submarine fan at 8.2-5.5 Ma from onshore Hanoi Depression to Central Yinggehai-Song Hong Depression. (d) Distribution of the Red River delta and submarine fan in the northwest corner of the South China Sea. Dash lines show the distribution of the shelf breaks in the late Miocene in the Yinggehai-Song Hong and Qiongdongnan basins. YGH-SH: Yinggehai-Song Hong basin, QDN: Qiongdongnan basin.

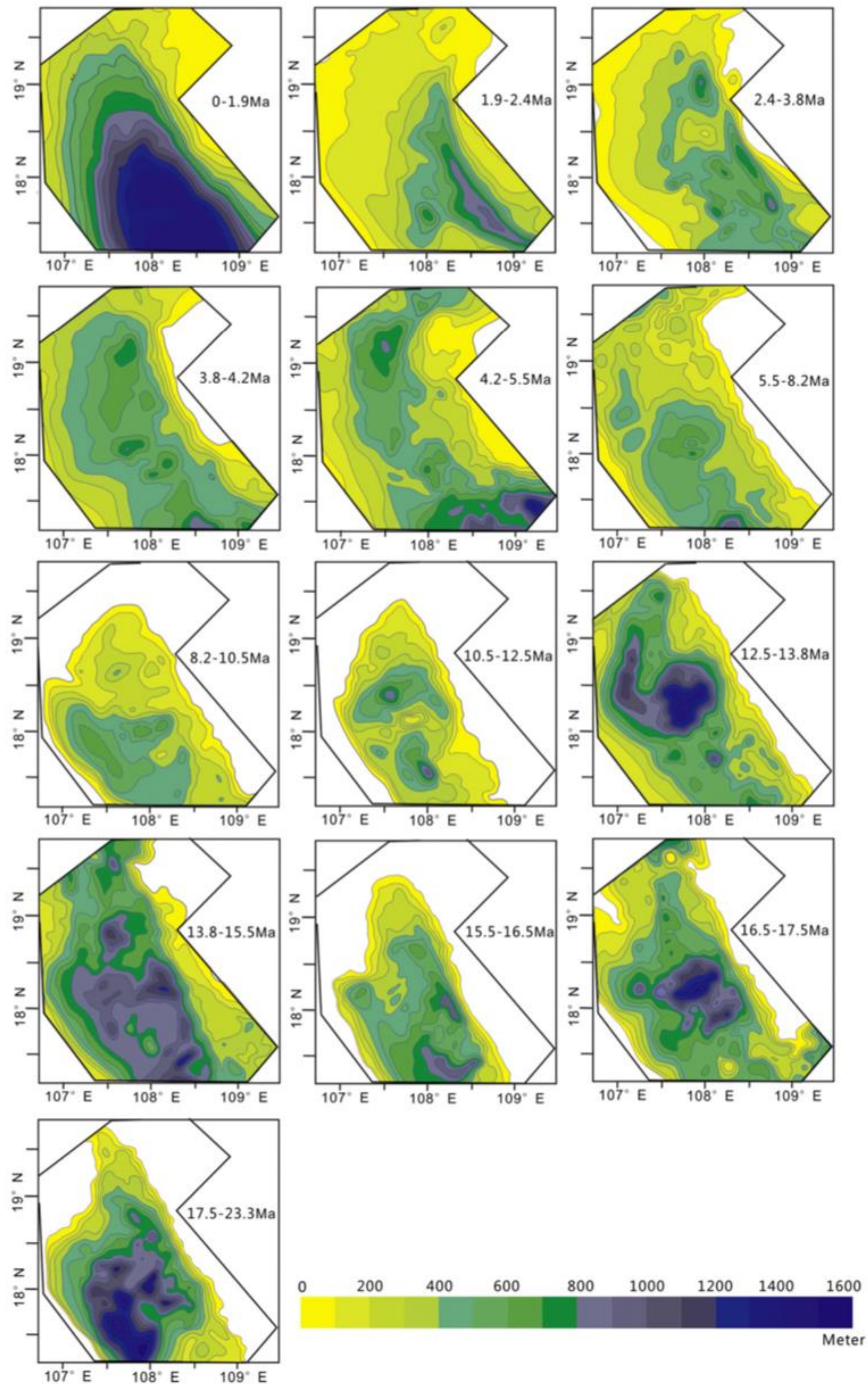
0-1.9Ma
1.9-2.4Ma
2.4-3.8Ma
3.8-4.2Ma
4.2-5.5Ma
5.5-8.2Ma
8.2-10.5Ma
10.5-12.5Ma
12.5-13.8Ma
13.8-15.5Ma
15.5-16.5Ma
16.5-17.5Ma
17.5-23.3Ma
19° N
18° N
107° E
108° E
109° E
0
200
400
600
800
1000
1200
1400
1600
Meter

Fig.7 Regional maps showing the sediment thickness variability during the thirteen time periods investigated in this study. Specific depositional units shown here represent the main input to the sediment released from Red River catchment.

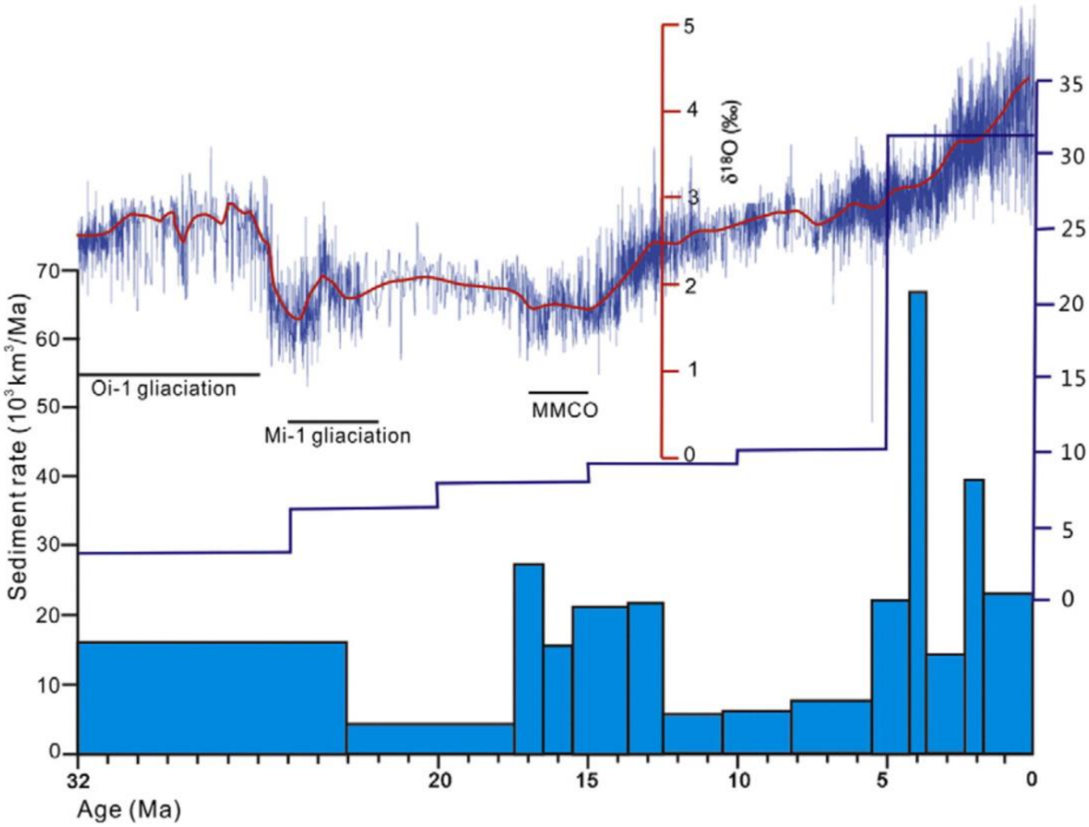

Fig.8 Estimated sediment volume accumulation rates since Oligocene for the Yinggehai-Song Hong basin (green block diagram). On the top of the figure, δ18O curve with scale bar in the middle indicates climatic shifts (Zachos et al., 2001) (red line). In the middle of the figure, blue line and values on the right axis indicate global sediment mass accumulation from Hay et al (1988) averaged over 5 Ma time intervals. MMCO: Mid-Miocene climatic optimum

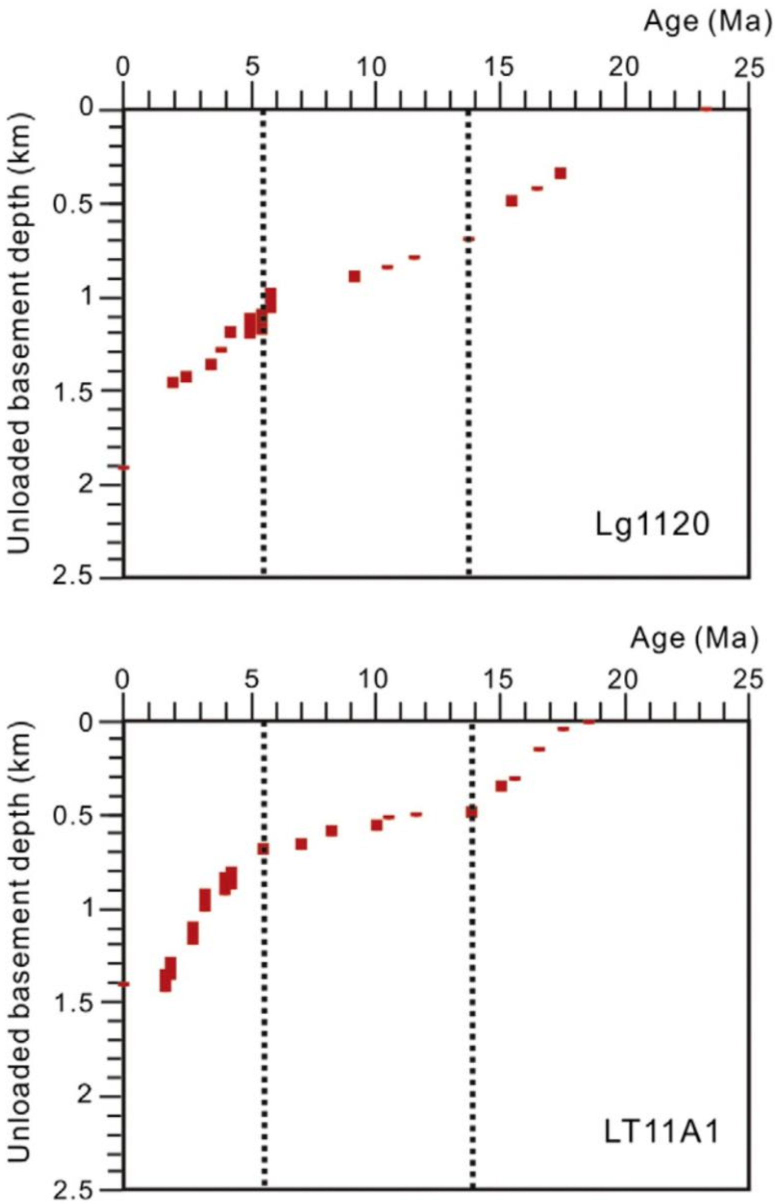

Fig. 9. Backstripped subsidence history of the sediment-unloaded basement at site of Well LG1120 in the Lingao Uplift and Well LT11A1 in the Central Yinggehai-Song Hong Depression. Red vertical bars indicate the unloaded depth to basement at each time, the length of the bar showing uncertainties derived from paleo-water depth.

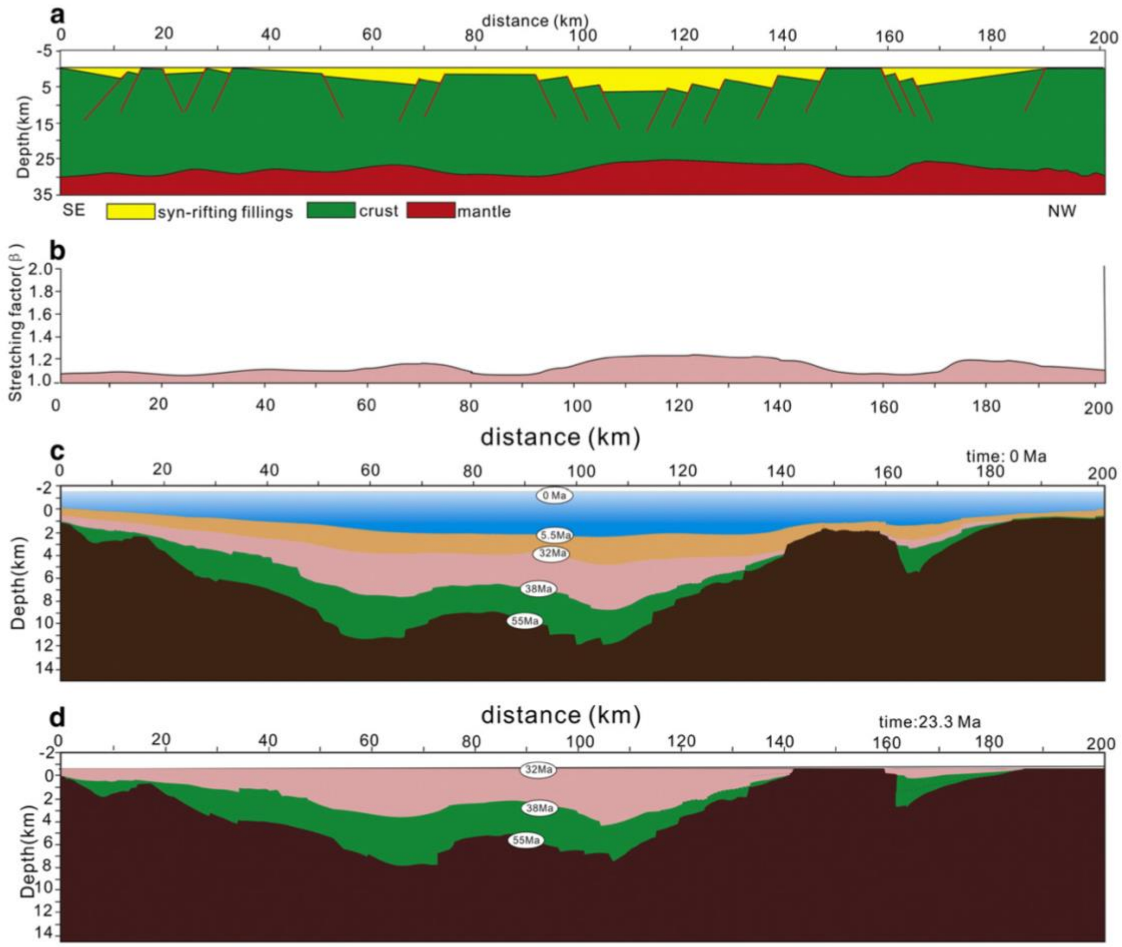

Fig. 10 Depth-dependent lithospheric streching for line 0793 in the Yinggehai-Song Hong basin. (a) Syn-rift lithosphere response to extension along plannar faults in the upper crust showing half graben formation, footwall uplift and block rotation. (b) Variable upper crust stretching factors profile generated by forward model. (c) Present-day depth section of the Line 0793. (d) Section reverse modeled to 23.3 Ma with stretching factor profile, which is for whole-lithospheric stretching (e). (f) Stretching factor determined for upper, whole crust and whole lithosphere for Line 0793 in the Yinggehai-Song Hong basin.

Table 1 Lithology and age constraints taken from wells LG1120 and LT11A1, which are used for the 1D subsidence analysis

Depth (m)	Thickness (m)	Age (Ma)	Depositional environment	Minimum paleo-water depth (m)	Maximum paleo-water depth (m)	Litho 1	L1 (%)	Litho 2	L2 (%)	Litho 3	L3 (%)
LG1120											
446		0.00									
573	127	1.90	Littoral	1.00	20.00	Sand	0.53	Shale	0.47		
735	162	2.40	Littoral	1.00	20.00	Shale	0.63	Sand	0.37		
1050	315	3.40	Littoral	1.00	20.00	Shale	0.56	Sand	0.44		
1495	445	3.80	Littoral	1.00	20.00	Shale	0.58	Sand	0.42		
1675	180	4.00	Littoral	1.00	20.00	Shale	0.78	Sand	0.22		
1750	75	4.20	Littoral	1.00	20.00	Shale	0.91	Sand	0.09		
2075	325	5.00	Neritic	21.00	150.00	Shale	0.67	Sand	0.33		
2150	75	5.50	Neritic	21.00	150.00	Sand	0.52	Shale	0.48		
2320	170	5.80	Neritic	21.00	150.00	Shale	0.65	Sand	0.35		
2350	30	6.30	Littoral	1.00	20.00	Shale	0.64	Sand	0.36		
2520	170	9.20	Littoral	1.00	20.00	Shale	0.88	Sand	0.12		
2595	75	10.50	Coastal plain	0.00	1.00	Shale	0.97	Sand	0.03		
2675	80	11.60	Coastal plain	0.00	1.00	Shale	0.83	Sand	0.17		
2839	164	13.80	Coastal plain	0.00	1.00	Shale	0.85	Sand	0.15		
3272	433	15.50	Littoral	1.00	20.00	Sand	0.60	Shale	0.40		
3327	55	16.50	Coastal plain	0.00	1.00	Shale	0.80	Sand	0.20		
3475	149	17.50	Littoral	1.00	20.00	Shale	0.54	Sand	0.46		
3803	328	23.00	Coastal plain	0.00	1.00	Shale	0.53	Sand	0.47		
LT11A1											
51		0									
445	394	1.64	Neritic	21.00	150.00	Sand	0.53	Shale	0.47		
670	225	1.8	Neritic	21.00	150.00	Sand	0.54	Shale	0.46		
1270	600	2.7	Neritic	21.00	150.00	Shale	0.75	Sand	0.25		
1730	460	3.2	Neritic	21.00	150.00	Shale	0.66	Sand	0.34		
1900	170	4	Neritic	21.00	150.00	Shale	1.00	Sand	0.00		
1975	75	4.2	Littoral	1.00	20.00	Shale	1.00	Sand	0.00		
2100	125	5.5	Littoral	1.00	20.00	Shale	0.59	Sand	0.41		
2150	50	7	Littoral	1.00	20.00	Shale	1.00	Sand	0.00		
2250	100	8.2	Littoral	1.00	20.00	Shale	0.63	Sand	0.37		
2295	45	10	Littoral	1.00	20.00	Shale	0.74	Sand	0.26		
2335	40	10.5	Coastal plain	0.00	1.00	Shale	0.54	Sand	0.46		
2370	35	11.6	Coastal plain	0.00	1.00	Sand	0.54	Shale	0.46		
2430	60	13.8	Littoral	1.00	20.00	Sand	0.75	Shale	0.25		
2680	250	15	Littoral	1.00	20.00	Sand	0.74	Shale	0.26		
2724	44	15.5	Coastal plain	0.00	1.00	Sand	0.92	Shale	0.08		
2920	196	16.5	Coastal plain	0.00	1.00	Sand	0.59	Shale	0.41		
3010	90	17.5	Coastal plain	0.00	1.00	Shale	0.84	Conglomerate	0.09	Sand	0.07
3048	38	18.5	Littoral	1.00	20.00	Shale	0.58	Sand	0.28	Conglomerate	0.14